

The pseudo-Goldstone spectrum of 2-colour QCD at finite density.

J. B. Kogut and D. Toublan

*Dept. of Physics, University of Illinois,
1110 West Green Street, Urbana, IL 61801-3080, USA*

D. K. Sinclair

*HEP Division, Argonne National Laboratory,
9700 South Cass Avenue, Argonne, IL 60439, USA*

Abstract

We examine the spectrum of 2-colour lattice QCD with 4 continuum flavours at a finite chemical potential (μ) for quark-number, on a $12^3 \times 24$ lattice. First we present evidence that the system undergoes a transition to a state with a diquark condensate, which spontaneously breaks quark number at $\mu = m_\pi/2$, and that this transition is mean field in nature. We then examine the 3 states that would be Goldstone bosons at $\mu = 0$ for zero Dirac and Majorana quark masses. The predictions of chiral effective Lagrangians give a good description of the behaviour of these masses for $\mu < m_\pi/2$. Except for the heaviest of these states, these predictions diverge from our measurements, once μ is significantly greater than $m_\pi/2$. However, the qualitative behaviour of these masses, indicates that the physics is very similar to that predicted by these effective Lagrangians, and there is some indication that at least part of these discrepancies is due to saturation, a lattice artifact.

I. INTRODUCTION

Recently there has been a renewed interest in the properties of nuclear matter — hadronic matter at finite non-zero baryon number (and isospin) density [1, 2]. Much of this interest comes from a reevaluation of the old idea that quark pairs might condense giving rise to a transition to a colour superconducting state at high baryon-number density [3, 4]. These newer studies indicate that the energies associated with this transition are much larger than the original estimates so that they could have a significant effect on the equation-of-state of nuclear matter. Unfortunately, adding a finite chemical potential for quark/baryon number to the Euclidean QCD action renders the fermion determinant complex which precludes the naive application of standard lattice simulation methods. (Some advances have been made allowing studies at small chemical potential and high temperatures, but their ranges of applicability are limited [5].) For this reason people have turned to the study of models which have some of the properties of QCD at finite baryon number but have real, positive fermion determinants, allowing lattice simulations.

One such model is 2-colour QCD with fundamental quarks. With $SU(2)_{colour}$, the quarks and anti-quarks are in the same representation, leading to a fermion determinant which remains real and positive in the presence of a quark-number chemical potential, μ . It is expected that, at $\mu = m_\pi/2$, this model exhibits a phase transition to a state with a colourless diquark condensate which breaks quark number, and associated Goldstone bosons. Thus this condensed phase is a superfluid rather than a superconductor. Chiral effective Lagrangians have been used to predict the phase structure of this theory [6, 7, 8, 9, 10] as have random-matrix models [11].

This predicted phase structure including the mean-field nature of the transition has been observed in lattice simulations [12, 13, 14, 15, 16, 17, 18]. However, the only simulations in which it was possible to study the masses of potential Goldstone bosons were performed at a quark mass so large that it was difficult to measure those excitations which were significantly more massive than the pion [13]. It was also unclear at such large quark masses if the masses of these pseudo-Goldstone modes were well separated from the rest of the hadron spectrum. Since these earlier simulations were performed at a quark mass of $m = 0.1$, we have performed new simulations at the same $\beta(1.5)$ and quark mass $m = 0.025$ which should halve the pion mass m_π . These simulations were performed on a $12^3 \times 24$ lattice again with

the quark-number symmetry breaking parameter $\lambda = 0.1m$ and $\lambda = 0.2m$ to keep the explicit symmetry breaking, which depends on λ/m , small. We have also performed simulations on a smaller (8^4) lattice to give us some indication of the magnitude of finite size effects.

In these simulations which had a single staggered quark field corresponding to 4 continuum quark flavours, the lattice flavour symmetry at $m = \lambda = \mu = 0$ is $U(2)$. When this breaks spontaneously, $U(2) \rightarrow U(1)$ giving rise to 3 Goldstone bosons. We study the behaviour of these 3 states for $m \neq 0$, $\mu \neq 0$ and $\lambda \ll m$, and compare with the leading-order predictions from chiral effective Lagrangians. For $\mu < m_\pi/2$, the agreement with these predictions is excellent. As μ is increased beyond $m_\pi/2$, the mass of the excitation which would be a Goldstone boson for $\lambda = 0$ and that of the pion, lie consistently below the predictions from tree-level effective Lagrangians. Part of this difference might be due to higher order corrections in the effective Lagrangian calculations, which cannot be characterized by a single parameter in addition to those of tree-level chiral perturbation theory. However, at least some of this ‘discrepancy’ appears to be due to the fact that, at high densities, the fermionic constituents of these excitations are revealed, indicating that we are beyond the reach of chiral perturbation theory. However, the high density behaviour of the lattice theory is strongly affected by saturation, a lattice artifact, so it is unclear how much of this would survive to the continuum.

In section 2 we review the expected pattern of symmetry breaking for lattice 2-colour QCD with 1 fundamental staggered quark field (4 flavours), and the (pseudo)-Goldstone spectrum associated with this breaking. Throughout our analysis we compare the lattice results to analytical calculations derived from effective models. We use a non-linear-sigma model (chiral perturbation theory) at leading order similar to that described in [7], and a linear sigma model that models some of the higher order corrections to chiral perturbation theory. We present the linear sigma model effective Lagrangian we use to fit our diquark condensates, and its predictions for the pseudo-Goldstone spectrum in section 3, while, for completeness, the non-linear sigma model is presented in Appendix A. Section 4 describes our simulations, presents our results for the condensates and the evidence for mean-field scaling. In section 5 we present our measurements of the spectrum of this theory, and its comparison with the predictions of effective Lagrangian analyses. Our conclusions are presented in section 6.

II. SYMMETRY BREAKING IN 2-COLOUR LATTICE QCD

The staggered fermion action for 2-colour lattice QCD with 1-staggered fermion, i.e. 4 continuum flavours in the fundamental representation of the colour group is:

$$S_f = \sum_{sites} \left\{ \bar{\chi} [\mathcal{D}(\mu) + m] \chi + \frac{1}{2} \lambda [\chi^T \tau_2 \chi + \bar{\chi} \tau_2 \bar{\chi}^T] \right\} \quad (1)$$

where $\mathcal{D}(\mu)$ is the normal staggered covariant finite difference operator with links in the $+t$ direction multiplied by e^μ and those in the $-t$ direction by $e^{-\mu}$. What follows summarizes the analysis of the symmetries of this theory presented in detail in [12]

At $\mu = m = \lambda = 0$, this action has a $U(2)$ flavour symmetry which breaks spontaneously to $U(1)$. If it breaks forming a chiral condensate, $\langle \bar{\chi} \chi \rangle$, there will be 3 broken $U(2)$ generators and 3 Goldstone bosons, namely;

$$\begin{aligned} \mathbf{1} &\implies \bar{\chi} \epsilon \chi \\ \sigma_1 &\implies \chi^T \tau_2 \chi - \bar{\chi} \tau_2 \bar{\chi}^T \\ \sigma_2 &\implies \chi^T \tau_2 \chi + \bar{\chi} \tau_2 \bar{\chi}^T. \end{aligned} \quad (2)$$

If it breaks forming a diquark condensate, $\frac{1}{2} \langle \chi^T \tau_2 \chi + \bar{\chi} \tau_2 \bar{\chi}^T \rangle$, there will again be 3 broken generators and 3 Goldstone bosons,

$$\begin{aligned} \mathbf{1} &\implies \chi^T \tau_2 \epsilon \chi + \bar{\chi} \tau_2 \epsilon \bar{\chi}^T \\ \sigma_2 &\implies \bar{\chi} \chi \\ \sigma_3 &\implies \chi^T \tau_2 \chi - \bar{\chi} \tau_2 \bar{\chi}^T. \end{aligned} \quad (3)$$

If $\mu \neq 0$ and $m = 0$, the staggered fermion action 1 is invariant under $U(1) \times U(1)$, which is completely spontaneously broken by the diquark condensate. Therefore, only the 2 diquark states in equation 3 remain Goldstone bosons.

When $m \neq 0$, the chiral condensate forms and the 3 Goldstone bosons of equation 2 gain equal masses given by PCAC. As μ is increased from zero, the mass of the pion created by $\bar{\chi} \epsilon \chi$ remains constant, since it has zero quark number and does not feel the effect of the chemical potential. The energy and hence the mass of the diquark state created by $\bar{\chi} \tau_2 \bar{\chi}^T$ is increased to $m_\pi + 2\mu$ for diquarks propagating in the $+t$ direction. The mass of the forward propagating anti-diquark is decreased to $m_\pi - 2\mu$.

This latter mass vanishes at $\mu = m_\pi/2$, and it becomes a true Goldstone boson. This heralds the phase transition to a state in which quark-number is spontaneously broken by a diquark condensate, $\frac{1}{2}\langle\chi^T\tau_2\chi + \bar{\chi}\tau_2\bar{\chi}^T\rangle$. The Goldstone boson is created by the orthogonal linear combination, $\frac{1}{2}(\chi^T\tau_2\chi - \bar{\chi}\tau_2\bar{\chi}^T)$, which we note is just that Goldstone mode which is common to equations 2 and 3.

For $\mu > m_\pi/2$, it is useful to introduce the concept of a total condensate Σ_c such that:

$$\langle\bar{\chi}\chi\rangle = \Sigma_c \cos \alpha, \quad (4)$$

and

$$\frac{1}{2}\langle\chi^T\tau_2\chi + \bar{\chi}\tau_2\bar{\chi}^T\rangle = \Sigma_c \sin \alpha. \quad (5)$$

We then see that the heaviest of our 3 would-be Goldstone bosons will be that created by the operator

$$\frac{1}{2}(\chi^T\tau_2\chi + \bar{\chi}\tau_2\bar{\chi}^T) \cos \alpha - \bar{\chi}\chi \sin \alpha, \quad (6)$$

which has zero vacuum expectation value. For μ just above the transition, this is predominantly a diquark/anti-diquark state, while for μ large, it is predominantly the scalar σ/f_0 meson, as expected since m can be neglected. This state will be heavy since the scalar meson is not a Goldstone boson when $\mu > 0$, even when $m = 0$. Finally, the pseudo-scalar pseudo-Goldstone boson is created by the operator

$$\bar{\chi}\epsilon\chi \cos \bar{\alpha} - \frac{1}{2}(\chi^T\tau_2\epsilon\chi + \bar{\chi}\tau_2\epsilon\bar{\chi}^T) \sin \bar{\alpha} \quad (7)$$

where effective Lagrangians suggest $\bar{\alpha} = \alpha$, with α introduced in (4, 5). For μ small, this state is predominantly a pion, while for large μ it is predominantly a pseudoscalar diquark. Since this pseudoscalar diquark would be a Goldstone boson if $m = 0$, its mass should approach zero for large μ when m can be neglected.

When $\lambda \neq 0$, the remaining Goldstone boson becomes massive. For the details of this λ dependence and for the μ dependence of the heavier, would-be Goldstone modes above the transition, we must turn to effective Lagrangians and chiral perturbation theory.

III. LINEAR SIGMA MODEL EFFECTIVE LAGRANGIAN

For small pion mass m_π , μ and λ , we should be able to use chiral perturbation theory to parametrize the behaviour of the condensates, quark-number density and pseudo-Goldstone

spectrum of this theory, as was done in [6, 7]. A reworking of this analysis for the symmetries of the staggered quark action is presented in the appendix. However, we find that m_π , even for the lowest quark mass m we use, is too large for tree-level chiral perturbation theory to give a quantitative description of the physics of this system except a relatively low chemical potential. While next-to-leading order chiral perturbation theory calculations have been performed [8], these do not yet include spectrum calculations. Even the calculation of the order parameters has not been extended beyond the neighbourhood of the critical point at next-to-leading order.

We therefore introduce an alternative effective Lagrangian which incorporates at tree level some of the properties expected from an all-orders chiral perturbation theory calculation. First, it should have the same phase structure and critical exponents (mean field) as tree-level chiral perturbation theory, and a critical point at $\mu = m_\pi/2$. At $\lambda = 0$, the spectrum of pseudo-Goldstone bosons for $\mu < m_\pi/2$ should be that predicted in the previous section from fairly general arguments, and for $\mu > m_\pi/2$, it should have one massless Goldstone boson. The magnitude of the total condensate $\sqrt{\langle \bar{\chi}\chi \rangle^2 + (\frac{1}{2}\langle \chi^T \tau_2 \chi + \bar{\chi} \tau_2 \bar{\chi}^T \rangle)^2}$ is independent of μ in tree-level chiral perturbation theory, but depends on μ at next-to-leading order. Lattice results indeed indicate that the total condensate increases when μ increases. Therefore the total condensate should be allowed to vary. Such variation can be allowed if the magnitude of the condensate becomes a dynamical field. With the chiral perturbation theory Lagrangian, this would be a non-perturbative effect, since it involves producing a bound state. Modifying our Lagrangian to explicitly incorporate such excitations requires replacing the chiral Lagrangian which is of the non-linear sigma model class by the corresponding linear sigma model effective Lagrangian. Since we do not intend to use this Lagrangian beyond tree level, we do not have to face the problems of trying to formulate a chiral perturbation theory based on this Lagrangian [19]. The simplest Lagrangian of this form is

$$\mathcal{L}_{\text{eff}} = \frac{1}{2}\text{Tr}\nabla_\nu\Sigma_l\nabla_\nu\Sigma_l^\dagger - \frac{1}{2}v_0M_\pi^2\text{ReTr}\hat{M}_\phi\Sigma_l - \frac{1}{2}\zeta\text{Tr}\Sigma_l\Sigma_l^\dagger + \frac{1}{4}\xi\left(\text{Tr}\Sigma_l\Sigma_l^\dagger\right)^2. \quad (8)$$

We have used the same conventions as in [7]:

$$\begin{aligned} \nabla_\nu\Sigma_l &= \partial_\nu\Sigma_l - \mu(B_\nu\Sigma_l + \Sigma_l B_\nu^T), \\ \nabla_\nu\Sigma_l^\dagger &= \partial_\nu\Sigma_l^\dagger + \mu(B_\nu^T\Sigma_l^\dagger + \Sigma_l^\dagger B_\nu), \end{aligned}$$

$$\begin{aligned}
B_\nu &= \delta_{0\nu} \begin{pmatrix} 1 & 0 \\ 0 & -1 \end{pmatrix}, \\
\hat{M}_\phi &= \begin{pmatrix} i \sin \phi & \cos \phi \\ \cos \phi & i \sin \phi \end{pmatrix},
\end{aligned} \tag{9}$$

where $\tan \phi = \lambda/m$.

The field $\Sigma_l = (v + \sigma)\Sigma$ contains v , the minimum of the free energy of the linear sigma model, as well as the radial and transverse fluctuations around that minimum. The field σ describes the radial fluctuations around that minimum. The three pseudo-Goldstone modes are the transverse fluctuations around that minimum. They are the same as in chiral perturbation theory and are contained in the field Σ given by:

$$\Sigma = U\bar{\Sigma}U^T, \tag{10}$$

where

$$U = \exp\left(\frac{i\Pi}{\sqrt{2}v}\right) \quad \text{with} \quad \Pi = \begin{pmatrix} P_S & Q_R + iQ_I \\ Q_R - iQ_I & P_S \end{pmatrix}, \tag{11}$$

and

$$\bar{\Sigma} = \begin{pmatrix} i \sin \alpha & \cos \alpha \\ \cos \alpha & i \sin \alpha \end{pmatrix}, \tag{12}$$

corresponds to the minimum of the free energy. M_π is the pion mass in the presence of the Majorana quark mass λ ,

$$M_\pi^2 = \frac{\sqrt{m^2 + \lambda^2}}{m} m_\pi^2, \tag{13}$$

where m_π is the pion mass at $\lambda = \mu = 0$. The Lagrangian is written in such a way that the masses of the pseudo-Goldstone modes are given by M_π at zero chemical potential.

Under a local flavor transformation $V \in U(2)$, the different fields transform in the following way

$$\begin{aligned}
\Sigma &\rightarrow V\Sigma V^T \\
\hat{M}_\phi &\rightarrow V^* \hat{M}_\phi V^\dagger \\
B_\nu &\rightarrow V B_\nu V^\dagger - \frac{1}{\mu} V \partial_\nu V^\dagger.
\end{aligned} \tag{14}$$

At $\mu = 0$ and $\lambda = 0$, the minimum of the free energy corresponds to

$$v_0 = \sqrt{\frac{m_\pi^2 + \zeta}{2\xi}}. \quad (15)$$

In general, the minimum of the free energy is given by minimizing

$$\mathcal{E} = \xi v^4 - \zeta v^2 - 4\mu^2 v^2 \sin^2 \alpha - 2M_\pi^2 v_0 v \cos(\alpha - \phi). \quad (16)$$

Comparing this to the phenomenological effective potential,

$$\mathcal{E} = \frac{1}{4} R^4 - \frac{1}{2} a R^2 - \frac{1}{2} b \mu^2 R^2 \sin^2 \alpha - c m R \cos \alpha - c \lambda R \sin \alpha. \quad (17)$$

used in our earlier work and in the next section, we see that these are identical under the substitutions $v = \sqrt{b/2}R/2$, $\zeta = 4a/b$, and $\xi = 16/b^2$ provided the critical value of μ , $\mu_c = m_\pi/2$.

The minimization conditions for the \mathcal{E} of equation 16 are

$$\begin{aligned} v(2v\mu^2 \sin 2\alpha - v_0 M_\pi^2 \sin(\alpha - \phi)) &= 0 \\ v_0 m_\pi^2 \cos(\alpha - \phi) + v(\zeta - 2v^2\xi + 4\mu^2 \sin^2 \alpha) &= 0. \end{aligned} \quad (18)$$

The computation of the spectrum of the linear sigma model is similar to that for chiral perturbation theory given in the appendix. For this case the σ field mixes with both the Q -modes, but not with the P_S mode. The secular equation for the σ and the two Q -modes is given by the setting the determinant of the matrix

$$\begin{bmatrix} E^2 - \mathbf{p}^2 + \zeta - 6v^2\xi + 4\mu^2 \sin^2 \alpha & 4\mu^2 \sin 2\alpha & 4\mu E \sin \alpha \\ 4\mu^2 \sin 2\alpha & E^2 - \mathbf{p}^2 + \zeta - 2v^2\xi + 2\mu^2(1 + \cos 2\alpha) & 4\mu E \cos \alpha \\ 4\mu E \sin \alpha & 4\mu E \cos \alpha & E^2 - \mathbf{p}^2 + \zeta - 2v^2\xi + 4\mu^2 \end{bmatrix} \quad (19)$$

to zero. The dispersion relation for the P_S modes is

$$E^2 = \mathbf{p}^2 + \frac{v_0}{v} M_\pi^2 \cos(\alpha - \phi) \quad (20)$$

In order to get the masses of the different modes, the secular equation and the dispersion relation must be solved together with the minimization equations. The secular equation can be cast in a form more similar to that presented in [7], by making use of the relation

$$\zeta - 2v^2\xi + 4\mu^2 = -\frac{v}{v_0} M_\pi^2 \frac{\sin \phi}{\sin \alpha}, \quad (21)$$

which is a consequence of equations 18. With this form one can see explicitly that in the ordered phase for $\lambda = 0$, where $\phi = 0$ but $\sin \alpha \neq 0$, there is a true Goldstone mode.

IV. LATTICE SIMULATIONS AND SCALING

We have simulated lattice 2-colour QCD with 1 staggered quark field (4 continuum flavours) at finite quark-number chemical potential μ on 8^4 and $12^3 \times 24$ lattices at $\beta = 4/g^2 = 1.5$ (close to the β_c for $N_t = 4$) and quark mass $m = 0.025$ in lattice units. Simulations were performed with the explicit symmetry-breaking parameter, $\lambda = 0.0025, 0.005$ (and zero, for small μ). We used the hybrid molecular-dynamics algorithm, performing simulations of 2000 molecular-dynamics time units at each μ and λ with dt as small as 0.0016. The chiral and diquark condensates, the quark number density, and the spectrum of candidate pseudo-Goldstone bosons were measured.

The diquark condensate, $\frac{1}{2}\langle\chi^T\tau_2\chi + \bar{\chi}\tau_2\bar{\chi}^T\rangle$, is plotted for the larger lattice in figure 1a. This condensate is seen to be small for $\mu \lesssim m_\pi/2 = 0.19264(7)$, and rapidly increases close to $m_\pi/2$. In addition, the decrease with decreasing λ suggests that the condensate would vanish as $\lambda \rightarrow 0$ for $\mu \leq 0.15$, while for $\mu > 0.225$, the condensate appears destined to remain finite in this limit. These observations strongly suggest that there is a phase transition, somewhere in the range $0.15 < \mu < 0.225$. To quantify this observation, we have fitted the behaviour of these condensates to scaling forms suggested from effective chiral Lagrangians. The fits to the simplest form which comes from the tree level analysis of the chiral Lagrangian of the non-linear sigma model variety described in the appendix are poor – $\chi^2/d.o.f = 64$ — so we turn again to a form based on the tree level analysis of a Lagrangian of the linear sigma model class, as described in section 3, which allows the magnitude of the condensate to vary. We have had good experience with such a form in the past for quenched theories and for QCD at finite isospin chemical potential [20, 21]. The diquark condensate is fitted to the form

$$\frac{1}{2}\langle\chi^T\tau_2\chi + \bar{\chi}\tau_2\bar{\chi}^T\rangle = c R \sin \alpha, \quad (22)$$

which derives from equation 17 where R and α are given from the minimization conditions of the previous section. For later reference we note that the prediction for the chiral condensate is

$$\langle\bar{\chi}\chi\rangle = c R \cos \alpha \quad (23)$$

while the quark-number density is

$$j_0 = b \mu R^2 \sin^2 \alpha. \quad (24)$$

The constant c is defined in terms of the critical μ , μ_c , through

$$c = \frac{b \mu_c^2}{m} \sqrt{a + b \mu_c^2}, \quad (25)$$

which is equivalent to equation 15, provided $\mu_c = m_\pi/2$.

Our best fit to the form of equation 22 has $a = 0.662(14)$, $b = 0.736(13)$, $m = 0.02528(4)$, $\mu_c = 0.19299(9)$ and $\chi^2/d.o.f. = 5.4$, over the range $0 \leq \mu \leq 0.4$. μ_c is in good agreement with the measured value of $m_\pi/2 = 0.19264(7)$, while m is close to the value 0.025 used in our simulations, considering the quality of the fit. Since the χ^2 for this fit appears poor, we compare the fit with the measurements both on the $12^3 \times 24$ lattice which we used for the fit, and for the 8^4 lattice in tables I,II. While the difference between the 8^4 and

μ	$\lambda = 0.0025$		
	8^4	$12^3 \times 4$	fit
	$\langle \chi^T \tau_2 \chi \rangle$	$\langle \chi^T \tau_2 \chi \rangle$	$\langle \chi^T \tau_2 \chi \rangle$
0.000	0.0730(2)	0.07351(5)	0.07361
0.100	0.0979(3)	0.1001(1)	0.09991
0.150	0.1604(9)	0.1747(3)	0.17458
0.175	0.2448(17)	0.2847(6)	0.28645
0.200	0.3856(28)	0.4475(13)	0.44775
0.225	0.5109(44)	0.5606(13)	0.56438
0.250	0.5900(51)	0.6320(14)	0.63519
0.300	0.6615(44)	0.7075(16)	0.71084
0.400	0.7257(50)	0.7758(16)	0.77845
0.500	0.7410(46)	0.8098(17)	0.82255
0.600	0.7586(53)	0.8312(18)	0.86512
0.800	0.6590(45)		
0.900	0.4236(39)		
1.000	0.0293(1)		

TABLE I: The diquark condensate $\frac{1}{2} \langle \chi^T \tau_2 \chi + \bar{\chi} \tau_2 \bar{\chi}^T \rangle$ as a function of μ , for $\lambda = 0.0025$

$12^3 \times 24$ ‘data’ suggest that the finite size effects in the measurements on the larger lattice are small, they are almost certainly comparable with and probably larger than the statistical

μ	$\lambda = 0.005$		
	8^4	$12^3 \times 4$	fit
	$\langle \chi^T \tau_2 \chi \rangle$	$\langle \chi^T \tau_2 \chi \rangle$	$\langle \chi^T \tau_2 \chi \rangle$
0.000	0.1437(3)	0.1451(1)	0.14518
0.100	0.1902(5)	0.1936(2)	0.19316
0.150	0.2893(12)	0.3030(4)	0.30342
0.175	0.3826(19)	0.4077(8)	0.40704
0.200	0.4883(23)	0.5191(8)	0.51529
0.225	0.5820(29)	0.5962(9)	0.59698
0.250	0.6275(33)	0.6529(10)	0.65228
0.300	0.6963(33)	0.7193(12)	0.71715
0.400	0.7509(37)	0.7817(11)	0.78057
0.500	0.7795(38)	0.8162(12)	0.82395
0.600	0.7969(40)	0.8354(12)	0.86628
0.800	0.7078(33)		
0.900	0.4945(27)		
1.000	0.0584(2)		

TABLE II: The diquark condensate $\frac{1}{2}\langle \chi^T \tau_2 \chi + \bar{\chi} \tau_2 \bar{\chi}^T \rangle$ as a function of μ for $\lambda = 0.005$

errors and the discrepancies between the ‘data’ and the fits given in these tables, over the range of the fits. For this reason we consider the fits to the linear sigma model form to be acceptable, indicating that the system undergoes a second order transition with mean-field critical exponents at $\mu = m_\pi/2$. We have also shown the fit to the tree-level chiral perturbation theory mentioned above in our figure. While this clearly has a more limited range of validity, it does not appear that unreasonable over this range. However, in order to obtain this quality of fit, we were forced to use $m = 0.02632(2)$. This is far enough from the true mass $m = 0.025$ that, as we shall see, the prediction for the chiral condensate is considerably poorer.

Since this fit gives not only the μ and λ dependence but also predicts the m dependence, we have plotted the predictions of this fit for our old ‘data’ at $m = 0.1$ [13] in figure 1b. Considering the fact that $m = 0.1$ is rather large to expect fits aimed at the chiral limit to

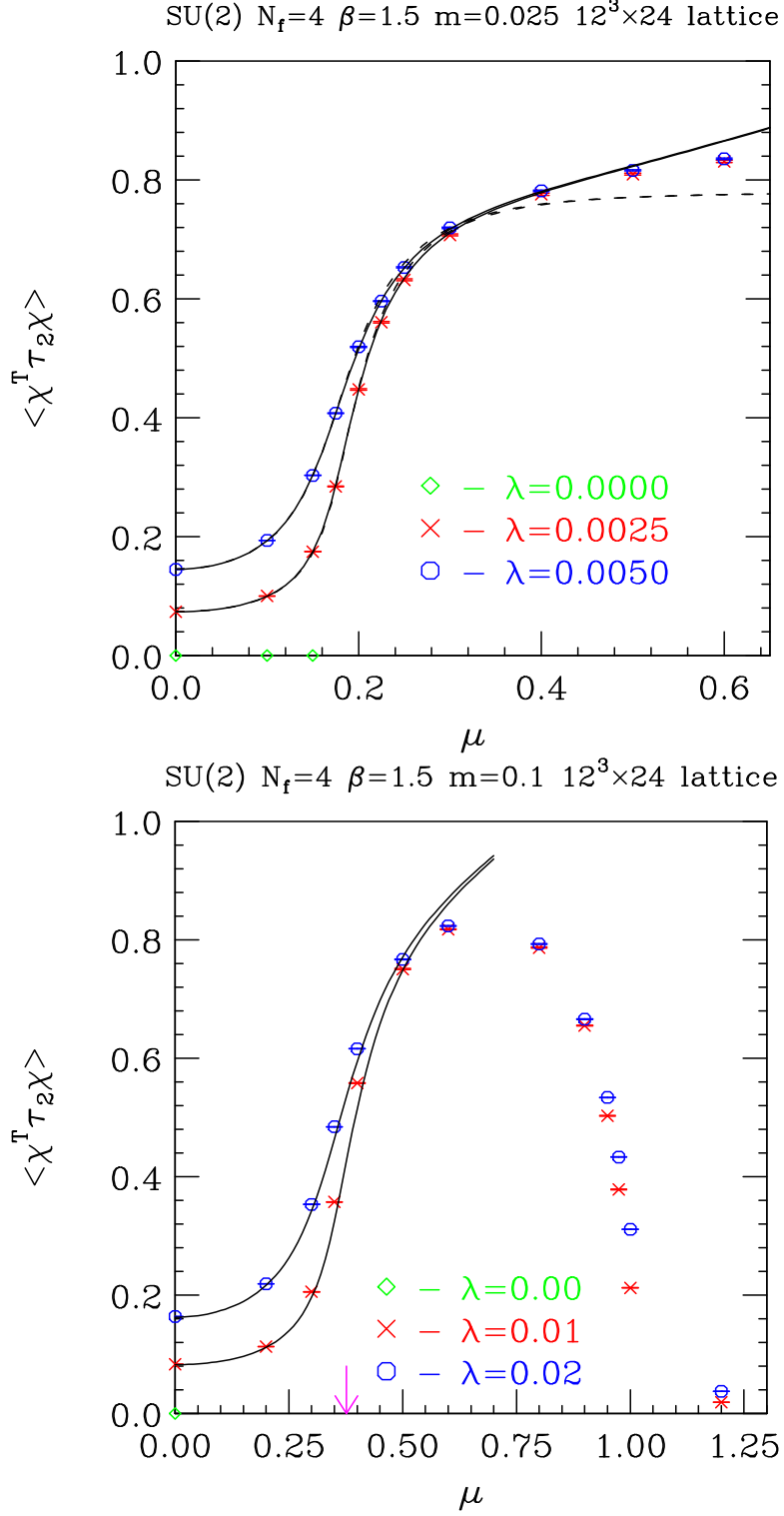


FIG. 1: The diquark condensate as a function of μ on a $12^3 \times 24$ lattice. The solid lines are fits to the form of equation 22. The dashed lines are fits to the chiral perturbation theory forms in the appendix. a) $m = 0.025$, b) $m = 0.1$.

work well, the prediction is remarkably good below $\mu = 0.6$ where the effects of saturation start to be seen.

On the smaller lattice we see that the diquark condensate has a broad peak near $\mu = 0.6$, beyond which it falls, remaining very small above $\mu \approx 1$. Since, as we shall see later, the quark-number density approaches 2, the maximum value allowed by fermi statistics, at these μ values, we interpret this fall as a saturation effect, a finite lattice spacing artifact. Further evidence that this is indeed a lattice artifact is found by comparing simulations at different lattice spacings. Comparing the results presented here at $\beta = 1.5$ with those at $\beta = 1.85$ [15] where the lattice spacing is about $2/3$ that at $\beta = 1.5$, we notice that the value of μ in lattice units where saturation is reached is consistent with being the same in both cases. In addition, the μ of the peak in the diquark condensate for $\beta = 1.85$ (in lattice units) is at least as large as at $\beta = 1.5$. If these were continuum effects the relevant lattice μ values for $\beta = 1.85$ would be smaller by roughly a factor of $2/3$, since $\mu = \mu_{physical}a$. Hence we conclude that the decrease in $\frac{1}{2}\langle\chi^T\tau_2\chi + \bar{\chi}\tau_2\bar{\chi}^T\rangle$ at large μ is purely a lattice artifact. Tables I,II indicate that finite size effects increase with μ , and that their effect is to depress the values of the condensate as μ increases. Thus we should expect that the infinite lattice peak will be at a higher μ value. However, it is probable that this value will still lie below the saturation μ , so that the falloff will occur over a range of μ , even on an infinite lattice, rather than as an abrupt discontinuity at the saturation value of μ . We come to this conclusion based on our experience with the quenched theory, where we have been able to examine the finite size effects more thoroughly [20].

In figure 2a we show the chiral condensate, $\langle\bar{\chi}\chi\rangle$, as a function of μ . As expected it remains approximately constant for $\mu < m_\pi$, above which it falls towards zero. The predictions of equation 23, using the parameters obtained from fits to the diquark condensates, are plotted on this graph. The agreement appears excellent over the scaling window. For comparison we include the predictions for $m = 0.1$ on our old ‘data’ at that mass. Here the agreement is considerably poorer. Presumably some of this is due to $m = 0.1$ being too high for these chiral effective Lagrangians. In addition, the chiral condensate is expected to be more sensitive to cutoff effects, such as saturation, at higher quark mass. Note that the prediction from the chiral perturbation theory fit mentioned above does relatively poorly, because this predicts that the magnitude of the total condensate is independent of μ which is not true. Thus by forcing this form to fit the diquark condensate, the prediction for the chiral

condensate must fail.

Finally we present the quark number density j_0 as a function of lattice μ in figure 3a for our $12^3 \times 24$ simulations. Since this data does not extend to the saturation region, we also plot the 8^4 ‘data’ in figure 4, along with the $\beta = 1.85$ results for comparison. Our corresponding ‘data’ from our old $m = 0.1$ runs is plotted, along with the predictions from equation 24, in figure 3b.

First we note that the $12^3 \times 24$ measurements start to depart from the predictions from our scaling form (equation 24) somewhat earlier than do either of the condensates, namely for $\mu > 0.3$. For $m = 0.025$, this does admit a small scaling window. For $m = 0.01$, since $0.3 < m_\pi/2$, there is no scaling window. The fact that the relevant variable appears to be μ rather than $2\mu/m_\pi$, suggests that at least some of this departure is a lattice artifact related to saturation.

As is observed in figure 4a, the quark-number density rises even more rapidly at larger μ , until it saturates at 2 near $\mu = 1$. Comparing these $\beta = 1.5$ measurements with those at $\beta = 1.85$ (figure 4b) indicates that saturation occurs at approximately the same μ in lattice units, confirming that saturation is a lattice artifact. However, j_0 would reach saturation at the same lattice μ independent of lattice spacing, if $j_0 \propto \mu^3$, at large μ . This is precisely the behaviour expected at large μ in the continuum. (This was pointed out by Son and Stephanov for QCD at finite isospin density [22].) The linear rise in the diquark condensate at large μ , which is a property of the linear-sigma-model fitting forms does predict a cubic rise in j_0 , but in every case we have considered the measured j_0 far exceeds our predictions. The hint that this might be real, i.e. not completely attributable to saturation, comes from the observation that the onset of this rapid rise in j_0 with μ appears to occur at a larger value of μ in lattice units at $\beta = 1.5$ (figures 3b,4a) than at $\beta = 1.85$ (figure 4b). This is what would be expected if it is a real effect rather than a lattice artifact. This earlier departure from the predictions from our tree-level analysis of our effective Lagrangian should not come as too much of a surprise. This analysis parametrizes the departure from tree-level chiral perturbation theory by a single new parameter. This parameter is set by our fit to the diquark condensate. Our new Lagrangian retains the same relationship between the diquark condensate and the density as the chiral perturbation theory Lagrangian. What we are seeing is evidence that this relationship breaks down at a μ value considerably less than the saturation value. To retain agreement beyond this point would require more

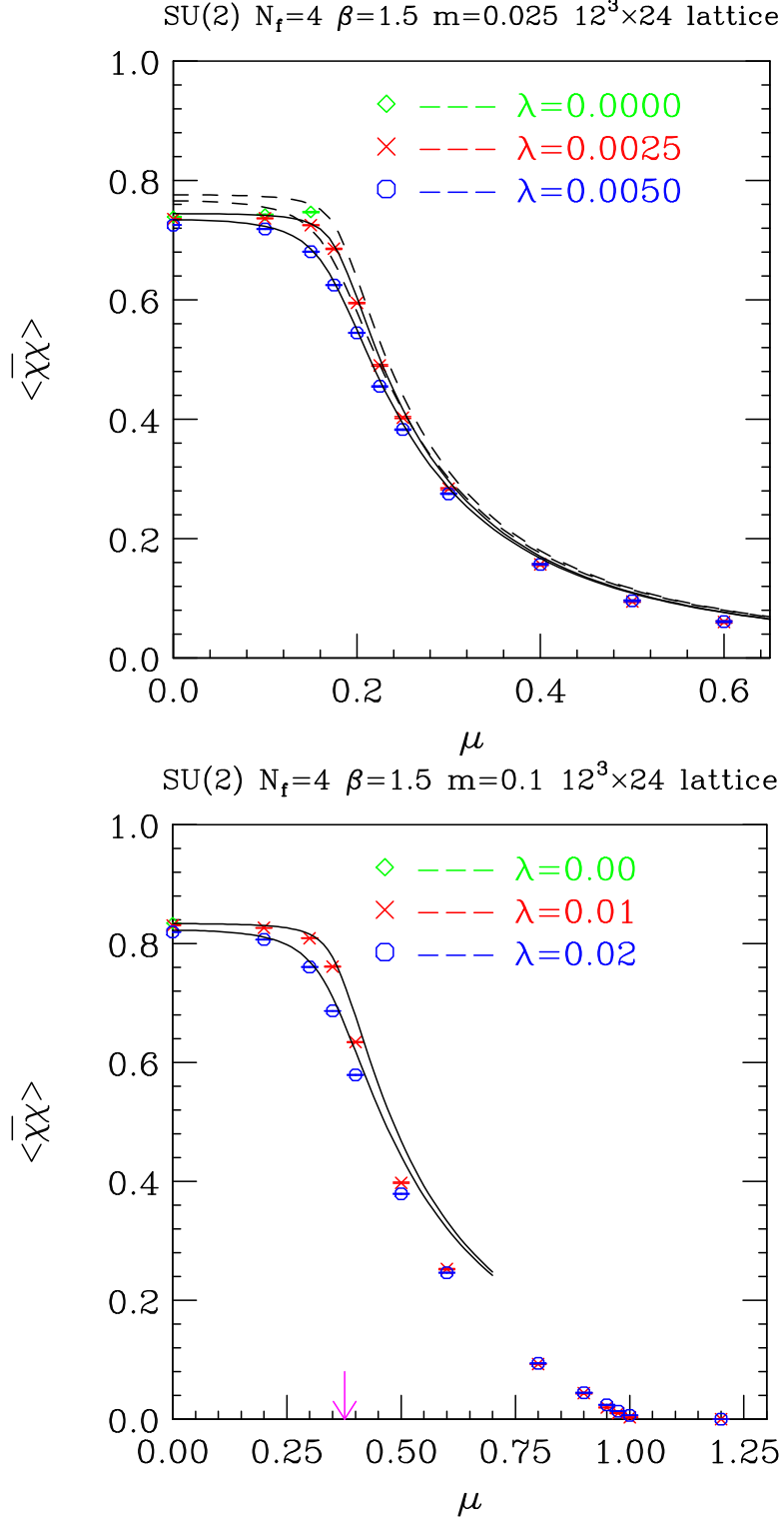


FIG. 2: The chiral condensate as a function of μ on a $12^3 \times 24$ lattice. The solid lines are from the fits to the diquark condensate. The dashed lines are the predictions of the fit to the tree-level chiral perturbation theory form. a) $m = 0.025$, b) $m = 0.1$.

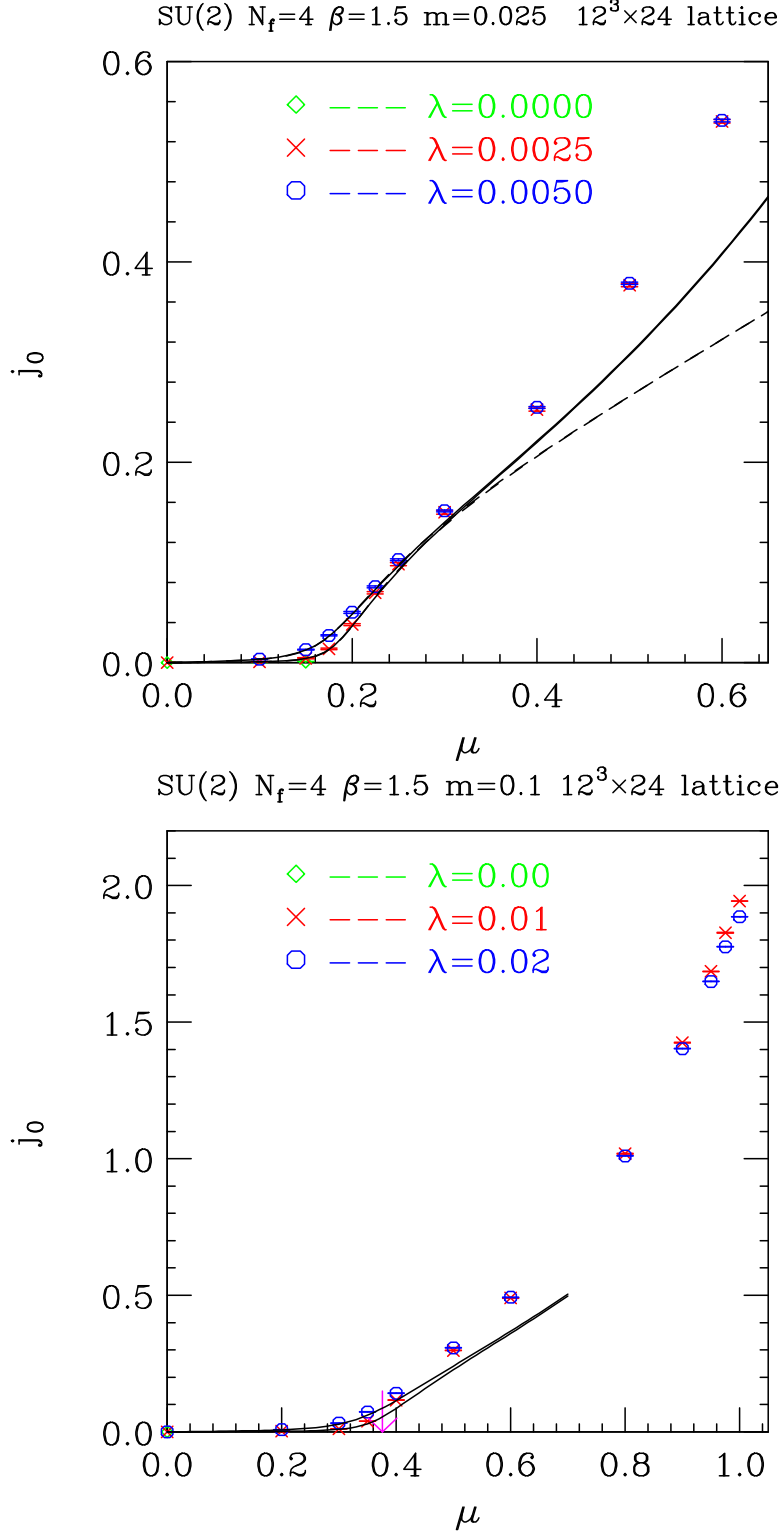


FIG. 3: The quark-number density j_0 as a function of μ at $\beta = 1.5$, $m = 0.025$ on a $12^3 \times 24$ lattice. The solid curves are the predictions from equation 24. The dashed curves are from tree-level chiral perturbation theory. a) $m = 0.0025$ b) $m = 0.1$.

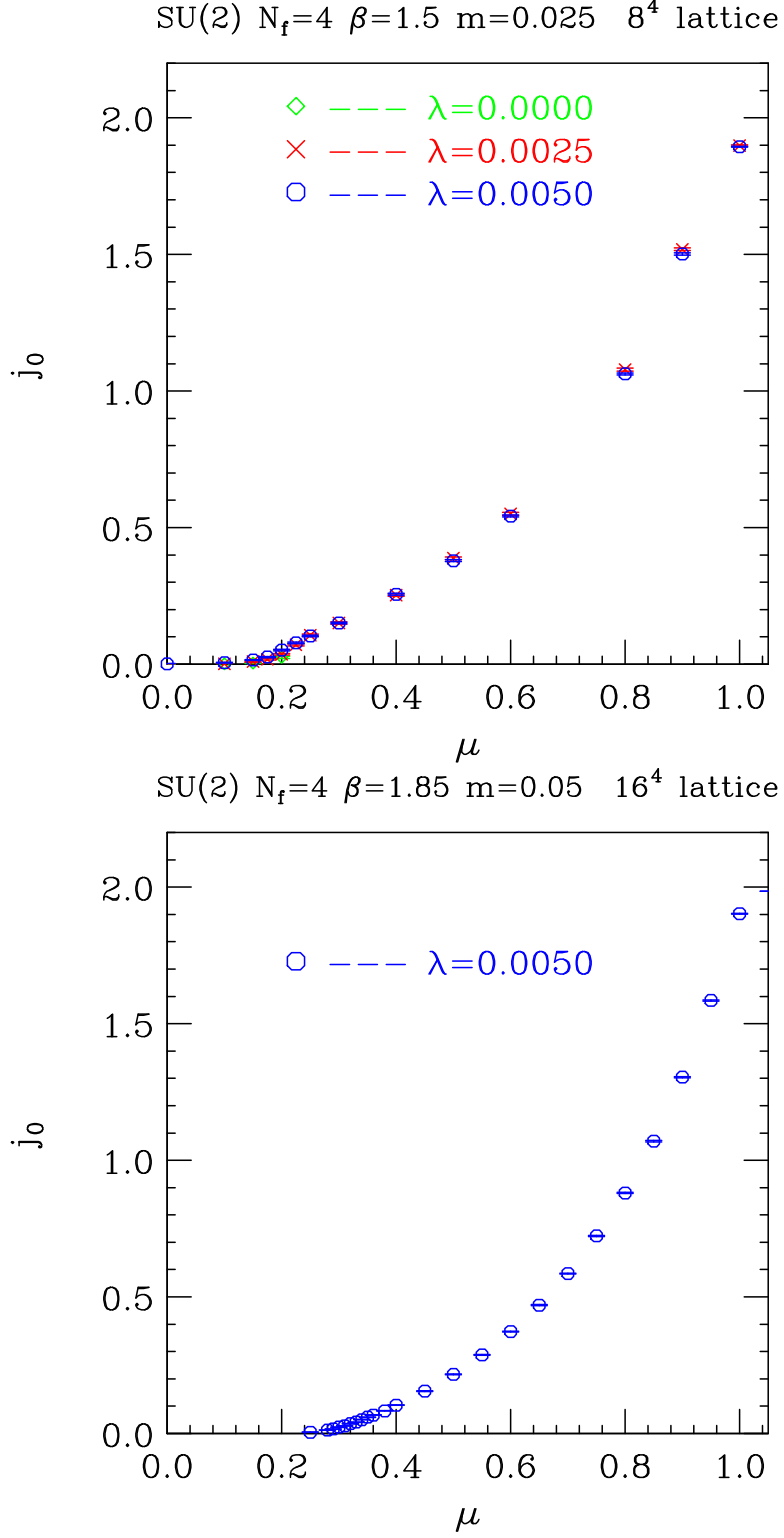


FIG. 4: The quark-number density j_0 as a function of μ at $\beta = 1.5$, $m = 0.025$ on a $12^3 \times 24$ lattice. The curves are the predictions from equation 24.

terms/parameters in our effective Lagrangian.

V. THE PSEUDO-GOLDSTONE SPECTRUM

As discussed in section 2 and made quantitative in section 3, spontaneous breaking of the lattice $U(2)$ flavour symmetry at $m = \mu = \lambda = 0$ should give rise to 3 Goldstone bosons. When these parameters are small, but non-zero, these excitations become pseudo-Goldstone bosons, gaining masses dependent on the magnitude of these symmetry-breaking parameters. We have measured the connected and disconnected contributions to the propagators of all local scalar and pseudoscalar diquarks in our $12^3 \times 24$ runs every 1 molecular-dynamics time step. The connected propagators are measured using noisy estimators of a point source on each odd respectively even site/colour of 1 time-slice of the lattice. The disconnected propagators are calculated using 5 sets of noisy sources defined over the whole odd respectively even sublattice, and the noise-diagonal terms are discarded.

The first state considered is the scalar diquark created by applying the operator $\frac{1}{2}(\chi^T \tau_2 \chi - \bar{\chi} \tau_2 \bar{\chi}^T)$ to the vacuum. For $\lambda = 0$ this will be a true Goldstone boson in the diquark condensed phase. With the small λ s we consider, it should have a small mass in the broken phase. Tree-level analysis of the chiral perturbation theory Lagrangian discussed in the appendix predicts that, at finite λ its mass should be given by equation A7 for the state labeled \tilde{Q} . Note that at $\lambda = 0$, this reproduces the predictions of simpler arguments $m_G = m_\pi - 2\mu$ for $\mu < m_\pi/2$ and zero for $\mu > m_\pi/2$. For the linear sigma model approach of section 3 this is replaced by the lowest lying solution of the secular equation obtained from equation 19. At $\lambda = 0$ the 2 forms are identical.

We fit our measured propagators P_G to the form

$$P_G(t) = A\{\exp[-m_G t] + \exp[-m_G(N_t - t)]\} \quad (26)$$

giving the results shown in figure 5a. The solid curves in this figure are the predictions from equation 19. The dashed curves are from equation A7. What we see is that equation 19 describes the decrease in mass of this would-be Goldstone boson well for $\mu < m_\pi/2$, and the dip near the transition value $m_\pi/2$. As μ is increased much beyond $m_\pi/2$, the ‘data’ falls below these predictions. These linear sigma model predictions are a considerable improvement over those of tree level chiral perturbation theory. This gives us confidence, that

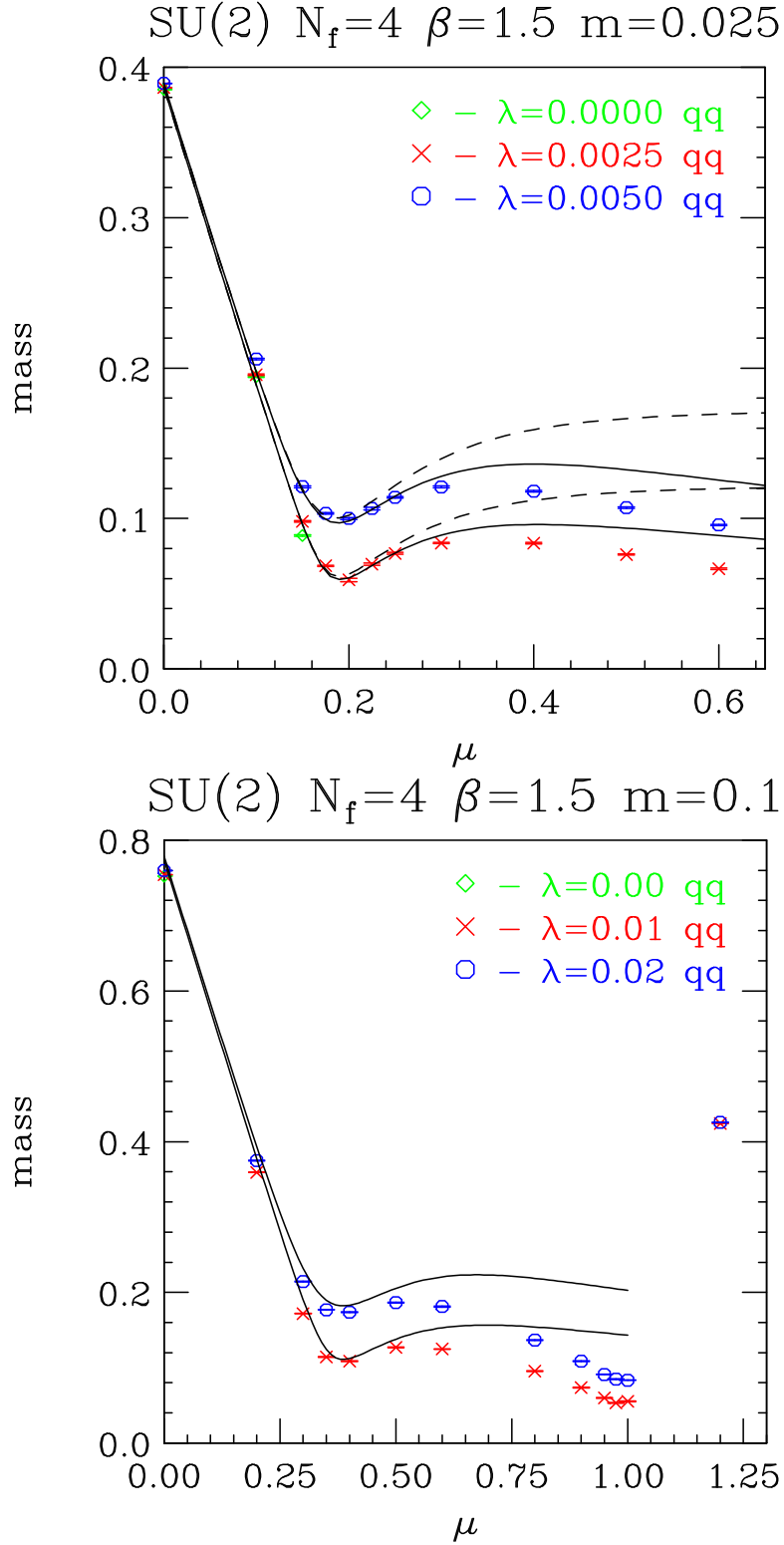


FIG. 5: The Goldstone boson of quark-number violation as a function of μ . a) $m=0.025$, b) $m=0.1$. The solid curves are the predictions from our fits. The dashed curves are from tree-level chiral perturbation theory.

even though these fits fail above the transition, this excitation will still have the expected behaviour in the limit $\lambda \rightarrow 0$, indicating that there is a phase transition to a state with a diquark condensate, and that this state is the massless Goldstone boson associated with the spontaneous breaking of quark number. In figure 5b we compare our predictions with our earlier measurements at $m = 0.1$, and find the agreement to be somewhat worse than at $m = 0.025$.

Such departures from the predictions of the linear-sigma-model form could well indicate that this model of the higher order terms in chiral perturbation theory is too naive to correctly predict more than the qualitative nature of the pseudo-Goldstone spectrum. The worse agreement for $m = 0.1$, where in terms of the scaling variable $x = 2\mu/m_\pi$ saturation occurs much sooner, suggests that the deviation could be largely due to saturation.

Next we turn to the consideration of the pseudoscalar pseudo-Goldstone boson. As described in section 2 and in particular in equation 7, at $\lambda = 0$ this is expected to be the pion for $\mu < m_\pi/2$. Above this value it mixes with the pseudoscalar diquark. For large μ it should be predominately a pseudoscalar diquark. Since the mixing angle $\bar{\alpha}$ in equation 7 is not known, beyond the predictions of effective Lagrangians which suggest that $\alpha = \bar{\alpha}$, we choose to fit the pion and pseudoscalar diquark propagators separately to a form analogous to that which we used for the Goldstone propagator. The graphs of the measured masses are presented in figures 6,7. We note that these masses have the expected behaviour in that they remain flat from $\mu = 0$ to the vicinity of $m_\pi/2$, and then commence to fall, becoming small for large μ where they should equal the masses of the would-be Goldstone boson. As expected these 2 estimators for the mass of the pseudoscalar pseudo-Goldstone boson, are in good agreement.

The effective (chiral) Lagrangian analysis presented in the appendix predicts that this pseudoscalar boson should have a mass given by the P_S state of equation A7, while our linear-sigma model form is given in equation 20. We have plotted these curves on our ‘data’ in figures 6a,7a. Although these predictions have qualitatively the same form as the ‘data’, clearly there is no quantitative agreement. (Note that the linear sigma model form of section 3 gives a slightly better fit than the chiral perturbation theory form in the appendix.) The form of the mass of equation 20 suggests that we compare our data with that of our earlier paper where $m = 0.1$. This we do in figures 6b,7b. Again we find the falloff in mass above $m_\pi/2$ is much more rapid for $m = 0.1$ than for $m = 0.025$. This comparison

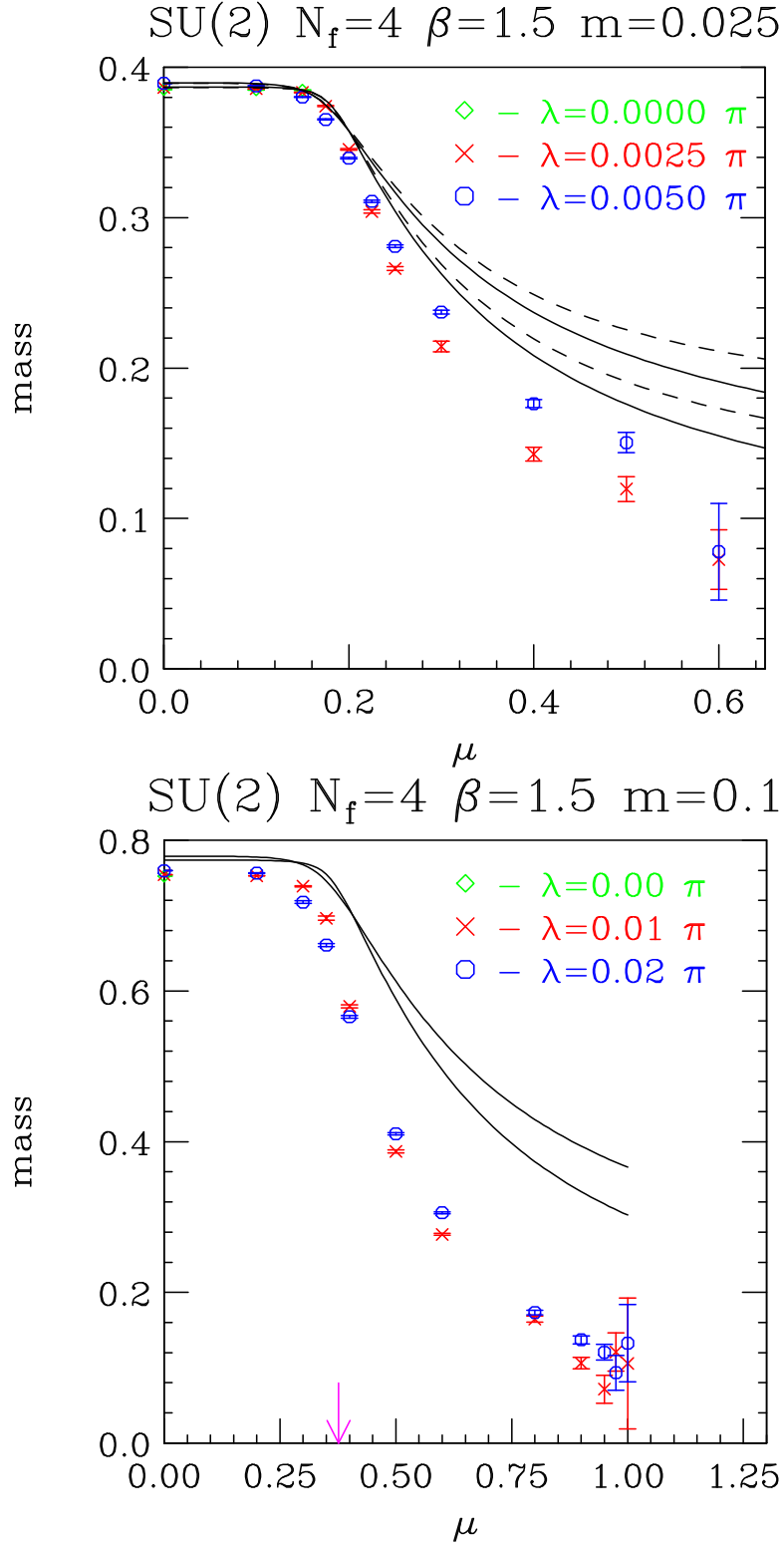


FIG. 6: The pion mass as functions of μ , on a $12^3 \times 24$ lattice at a) $m = 0.025$, b) $m = 0.1$. The curves are the scaling predictions mentioned in the text.

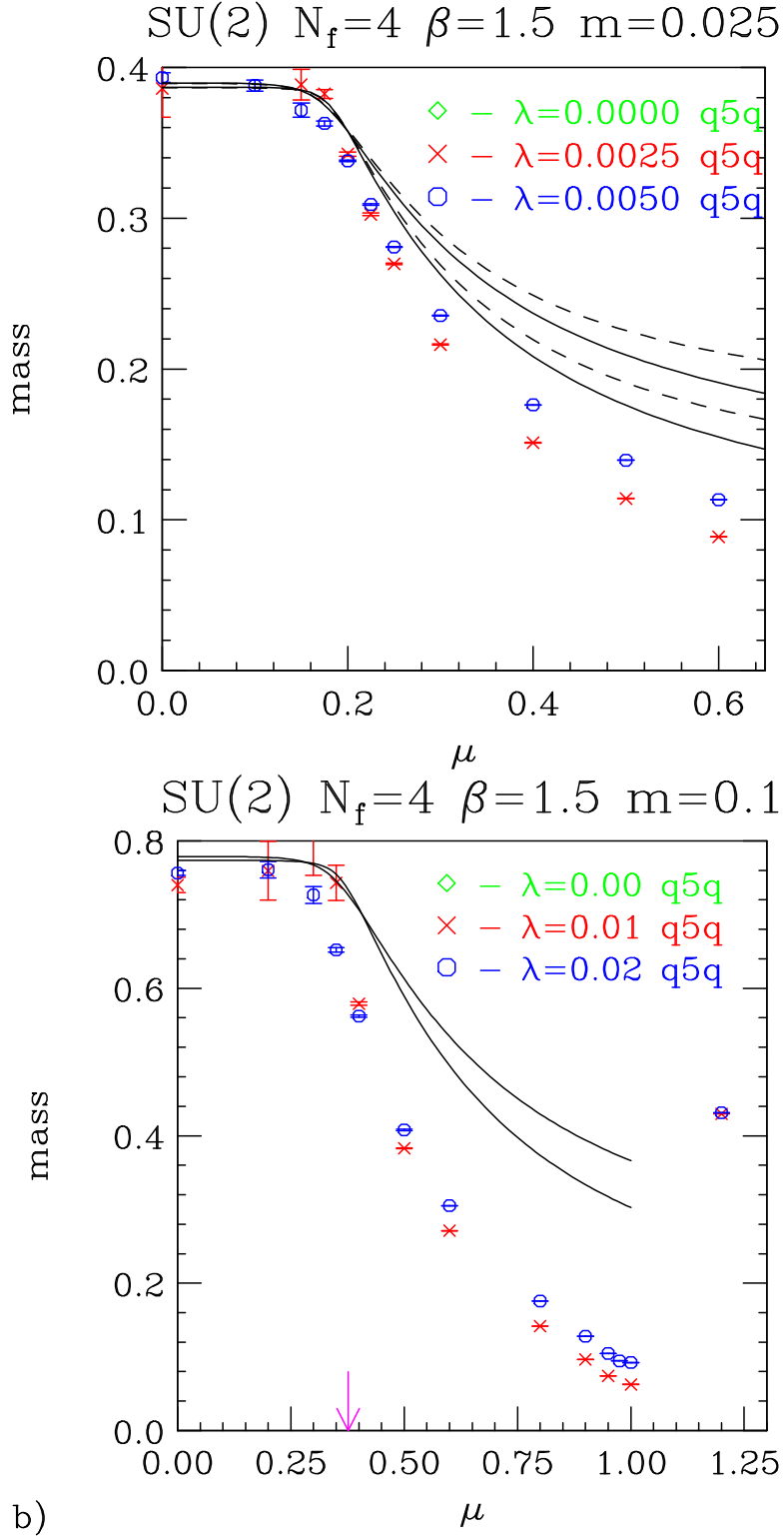


FIG. 7: The pseudoscalar diquark mass as functions of μ , on a $12^3 \times 24$ lattice at a) $m = 0.025$, b) $m = 0.1$. The curves are the scaling predictions mentioned in the text.

suggests that at least some of this is the effect of saturation, but if it is all a saturation effect, the range over which saturation has an effect is large. Any discrepancy between the measurements and fits which remains after removal of the effects of saturation should again be taken as an indication that our linear sigma model effective Lagrangian is inadequate to describe all departures from tree-level chiral perturbation theory.

We note that the term in each of our effective Lagrangians which relates j_0 to the diquark condensate is the term proportional to μ^2 . As we see in equation A6 of the appendix and its equivalent for the linear sigma model, this term also contributes to the masses of the pseudo-Goldstone bosons. Thus deviations of j_0 from our predictions, should imply differences in the pseudo-Goldstone boson masses from our predictions. The contribution to the state which is a true Goldstone boson at $\lambda = 0$, is proportional to $\sin^2 \alpha$, while that for the pseudoscalar is proportional to $\cos^2 \alpha$. Since α rises from zero above $\mu = m_\pi/2$, we would expect any departure from our predictions to occur earlier for the pseudoscalar than for the would-be Goldstone boson, which is precisely what we see.

The third pseudo-Goldstone boson is also a scalar state. It is the linear combination of the scalar diquark state and the flavour-singlet scalar meson given in equation 6. Here α is unambiguously defined by the requirement that this state has zero vacuum-expectation value, so we have calculated the propagator for this state. For $\mu < m_\pi/2$ and $\lambda = 0$ this state is a pure diquark state whose propagator is identical to that of the Goldstone state. Thus we will find both the Goldstone excitation and the state we want in this propagator. This will also remain true at finite λ . Since for finite λ , there is no phase transition in going from $\mu < m_\pi/2$ to $\mu > m_\pi/2$, it follows that these 2 states continue to mix above the transition, although the mixing becomes small for $\mu \gg m_\pi/2$. For this reason we fit our propagator to the form

$$P_S(t) = A\{\exp[-m_G t] + \exp[-m_G(N_t - t)]\} + B\{\exp[-m_S t] + \exp[-m_S(N_t - t)]\} \quad (27)$$

where $m_S > m_G$ is the mass of this scalar state, in addition to the form with $A = 0$, which is appropriate to the $\mu = 0$ propagator where $m_G = m_S$ and to $\mu \gg m_\pi/2$ where the lower lying state decouples. For μ small but non-zero, we extract this mass by fitting the propagator of the diquark state obtained by applying the operator $\bar{\chi}\tau_2\bar{\chi}^T$ to the vacuum, to the form

$$P_{qq} = A\{\exp[-m_S t] + \exp[-m_G(N_t - t)]\}. \quad (28)$$

This is obtained from the observation that for a pure diquark state (as opposed to a mixture of a diquark and an antidiquark) at $\lambda = 0$, the effect of the chemical potential is to add 2μ to the effective mass for propagation forward in time and subtract 2μ from the effective mass for propagation backward in time, thus separating the 2 scalar excitations. The masses obtained from these fits are plotted in figure 8.

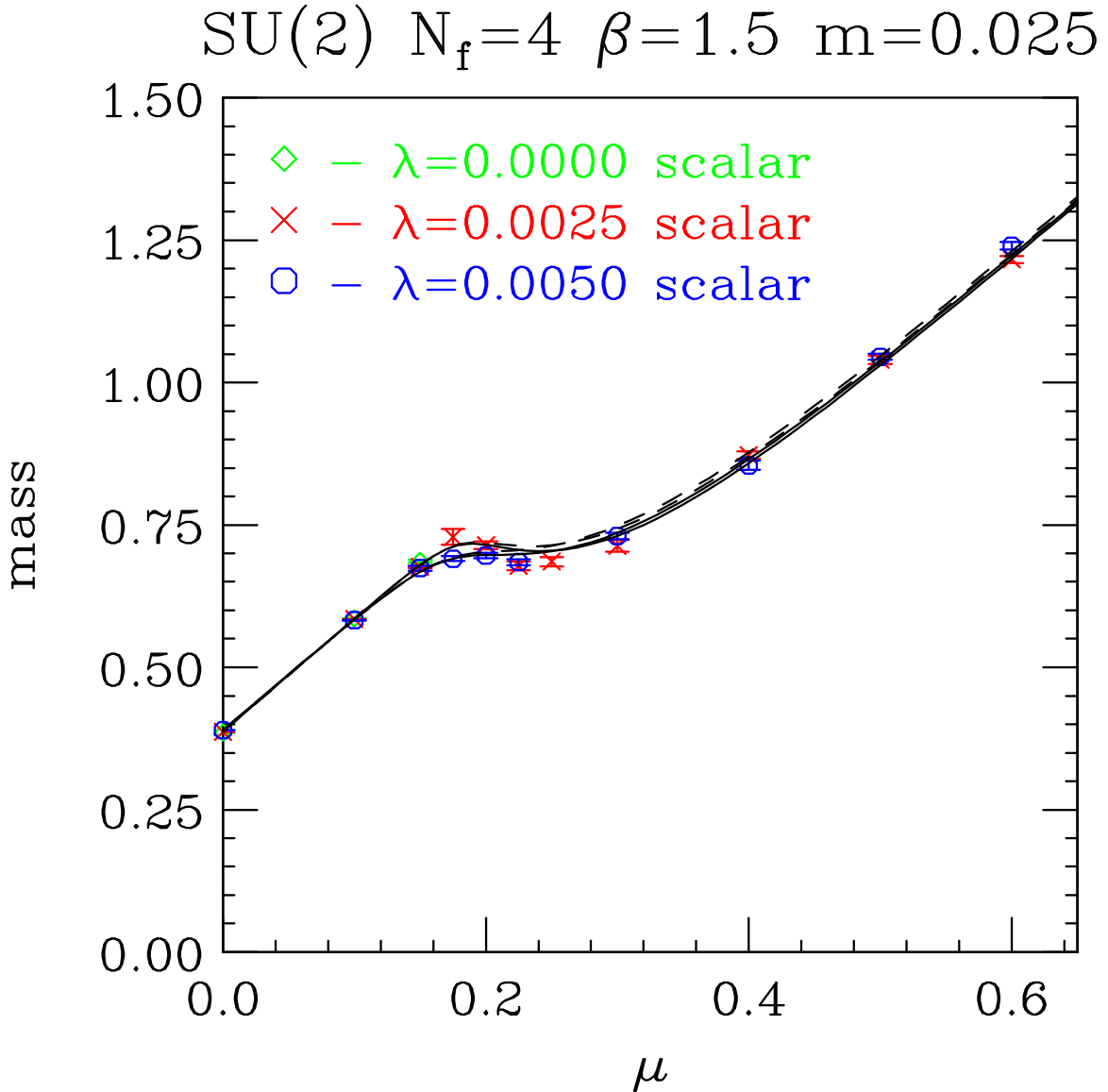


FIG. 8: The scalar mass as functions of μ , on a $12^3 \times 24$ lattice at $m = 0.025$. The curves are the scaling predictions mentioned in the text.

The analysis of section 3, predicts this mass to be the middle mass obtained from solving the secular equation 19, while the corresponding prediction from chiral perturbation theory

is the mass of \tilde{Q}^\dagger given in equation A7 of the appendix. We show these predictions on the ‘data’ of figure 8. The agreement is quite good, in contrast to the other 2 masses. In the low μ regime, the mass increases as $m_\pi + 2\mu$, as expected from general arguments. Just above m_π the mass shows a dip past which it resumes its increase, eventually becoming linear again with the same slope but zero intercept. Remembering that for $m = 0.1$, these masses should be roughly twice those presented here for $m = 0.025$, it is easy to see why they were too difficult to measure with any precision at that higher quark mass.

Finally we should mention the radial excitation. Even at $\lambda = 0$, its mass is > 2.76 for all μ . Since this is close to the momentum cutoff (π) on the lattice, it is not even clear if this should be considered as a real state. In any case, this mass is too high to be of more than passing interest.

VI. CONCLUSIONS

We have simulated 2-colour lattice QCD with one staggered fermion field corresponding to 4 continuum flavours, in the fundamental representation (doublet) of the colour group ($SU(2)$), at a finite chemical potential μ , and quark mass $m = 0.025$. As in previous simulations, we have observed the transition from the normal state to one characterized by a diquark condensate which spontaneously breaks quark-number. We have found that the equation-of-state, which describes the dependence of the diquark and chiral condensates on μ and the explicit symmetry breaking parameter λ , is well approximated by the tree-level approximation to a chiral Lagrangian in the linear sigma model class. The critical scaling implied by this analysis indicates that the transition is second order with mean-field critical exponents, as expected from chiral perturbation theory analyses through next-to-leading order. The measured critical value of μ is consistent with $m_\pi/2$ as expected. Applying the predictions of these fits to our earlier simulations at $m = 0.1$ we see evidence that our equation-of-state also gives a reasonable description of the mass dependence of these condensates. However, it is clear that saturation effects (a lattice artifact) limit the range of applicability of this equation for the higher mass, and we suspect that $m = 0.1$ might well be close to the limit of applicability of this approximation to chiral perturbation theory, if not to the applicability of chiral perturbation theory itself.

Our equation-of-state also predicts the μ , λ and m dependence of the quark-number

density. Here, it appears that the scaling window is somewhat narrower than that for the condensates. While the effect of saturation might explain why this density grows faster than the predictions for larger μ , we suspect that we are seeing the limitations of using tree-level results from an effective Lagrangian with only one more parameter than the leading order chiral perturbation theory Lagrangian, to model departures from tree-level chiral perturbation theory. Use of next-to-leading order chiral perturbation theory to fit our measurements would require going beyond what has already been done [8], and going beyond next-to-leading order would be extremely difficult. In addition, going to higher order in chiral perturbation theory introduces more parameters and thus reduces its predictive power. At high enough μ chiral perturbation theory will break down. The scale at which chiral perturbation theory breaks down is given by the pion decay constant F_π . From the numerous higher order calculations in chiral perturbation theory, this breakdown scale can be estimated to be of the order of a few times F_π . In our case at $\mu = 0$, we know the chiral condensate, the quark mass and the pion mass. From the Gell-Mann–Oakes–Renner relation, we find that $F_\pi \sim 0.25$. We therefore expect that chiral perturbation theory will break down when $\mu \sim 1$. However, at $\mu \sim 0.5$, higher-order corrections should already amount to 20 – 30%. We therefore conclude that it is very doubtful that chiral perturbation theory can describe our ‘data’ for the largest chemical potentials used in our study. Note that this F_π is the F_π for chiral perturbation theory with the lattice symmetries (see appendix). The continuum F_π is half this value.

Our large μ data suggests that j_0 is increasing consistent with the expected rise cubic in μ . Since the arguments leading to this prediction suggest a counting of degrees of freedom identical to that for free quarks, this suggests that we are beyond the range of chiral perturbation theory, since accounting for all these degrees of freedom in terms of hadrons requires including hadrons other than the pseudo-Goldstone bosons. Unfortunately it is difficult to disentangle such behaviour from the effects of saturation. A μ^3 increase in j_0 is just what is required to keep the saturation threshold at a constant μ in lattice units as the lattice spacing is varied, which is what we observe. In addition, the decrease of the condensate close to saturation, suggests that the quarks are acting like free quarks, which makes it even harder to distinguish real effects from saturation induced artifacts.

The main goal of this project was to measure the spectrum of pseudo-Goldstone bosons for this theory, to enhance our knowledge of the pattern of symmetry breaking. Spontaneous

breaking of the $U(2)$ symmetry of the staggered lattice implementation of 2-colour QCD with 1 staggered quark field corresponding to 4 continuum flavours at $m = \lambda = \mu = 0$, should give rise to 3 Goldstone bosons. Fixing $m = 0.025$, we have studied the variation of these now pseudo-Goldstone bosons as functions of μ for 2 choices of λ . Comparison with our earlier simulations at $m = 0.1$ gave some indication of the m dependence of these spectra. We have obtained the predictions from our linear sigma model effective Lagrangian for these masses, using the parameters obtained from our fits to the diquark condensate.

For $\mu = 0$ our measurements confirm that all 3 pseudo-Goldstone bosons are degenerate with mass consistent with the expected M_π . m_π is approximately proportional to \sqrt{m} as predicted by PCAC. The observed small deviations from PCAC suggest that $m = 0.1$ is beyond the range of the leading order prediction. At $\lambda = 0$, the lowest mass state is the diquark state orthogonal to the condensate. The mass of this state is expected to fall linearly to zero as μ is increased to $m_\pi/2$. Above this phase transition it should remain zero, becoming the Goldstone boson of spontaneously broken quark number. At small non-zero λ , our effective Lagrangian analysis predicts its behaviour. What we have observed is that these predictions are good up to and through the transition. As μ is increased much beyond this value, the measured mass lies consistently below these predictions. Examining the corresponding predictions for the higher quark mass $m = 0.1$, where the deviation is more severe, suggests that at least some of this deviation is coming from saturation, a lattice artifact seen when μ is large enough that the Fermi surface approaches the lattice cutoff.

When $\lambda = 0$, we expect that the pseudoscalar pseudo-Goldstone mass will remain constant as μ is increased up to $m_\pi/2$. Above this it is expected to decrease rapidly, approaching zero for large μ . Our measured values at $m = 0.025$ and non-zero λ show evidence for such behaviour. However, the rate of decrease in this mass above the transition is significantly faster than that predicted by the linear sigma model effective Lagrangian fits. At $m = 0.1$, this decrease is even more precipitous. Here again, there is evidence to suggest that this more rapid decrease is due to the effects of saturation. The improvement in going to the smaller mass, where the onset of saturation occurs at larger $x = 2\mu/m - \pi$, supports this interpretation, and suggests that if the mass were decreased, eventually the predictions would fit the ‘data’.

We have noted that the term in the effective Lagrangian which controls the behaviour of the quark-number density, also contributes to these pseudo-Goldstone masses, and does so in

a way which would be expected to make the discrepancies worse for the pseudoscalar state. Hence it is reasonable to assume that the addition of one extra parameter in going from the chiral perturbation theory Lagrangian to the linear sigma model Lagrangian, is inadequate to parameterize all departures from tree-level chiral perturbation theory. The behaviour of j_0 at high μ can be obtained from analyses other than those of effective Lagrangians. This suggests that one should abandon the use of effective chiral Lagrangians designed for small μ and small m_π and adopt a different approach for large μ .

At $\lambda = 0$, the final pseudo-Goldstone mass should increase linearly with μ up to $m_\pi/2$, above which it should briefly decrease before continuing its rise. We see evidence for this behaviour in our measurements for $m = 0.025$. The predictions from effective Lagrangians are in good agreement with the ‘data’ for this state.

We note that some of the other hadrons which could be expected to contribute at high μ , are those that would have been pseudo-Goldstone bosons were it not for the flavour symmetry breaking of the staggered lattice. On the lattice, the symmetry breaking is $U(2) \rightarrow U(1)$, giving 3 Goldstone bosons. In the continuum the symmetry breaking is $SU(8) \rightarrow Sp(8)$, which gives 27 Goldstone bosons.

To summarize, we have found $m = 0.025$ to be small enough to see evidence for mean-field scaling and to study the spectrum of the 3 pseudo-Goldstone excitations. At this quark mass, the pseudo-Goldstone boson masses lie well below those expected for other ‘hadrons’. However, saturation, where all available fermion levels are filled, is still close enough to the phase transition to make it difficult to disentangle real physics from this lattice artifact, even though we do find an adequate scaling region for simple observables. For $m = 0.1$ the scaling window is too small to obtain quantitative information. It would be useful to obtain the full next-to-leading order analysis of the pseudo-Goldstone spectrum, and the expressions for the order parameters beyond leading order in α . However, this is beyond the scope of this paper.

Acknowledgments

DKS is supported by the US Department of Energy under contract W-31-109-ENG-38. JBK and DT are supported in part by NSF grant NSF-PHY-0102409. DT is supported in part by “Holderbank”-Stiftung. These simulations were performed on the IBM SPs at

APPENDIX A: CHIRAL PERTURBATION THEORY AND THE GOLDSTONE SPECTRUM

In this appendix, we construct chiral perturbation theory for the symmetry breaking pattern of the staggered fermion action (1) at $m = \lambda = \mu = 0$: $U(2) \rightarrow U(1)$, and we study the spectrum of the three Goldstone excitations. These Goldstone modes become massive upon the introduction of a nonzero quark mass or a nonzero diquark source. They dominate the physics at low energy. In this appendix we study the spectrum in Chiral Perturbation Theory. This problem is similar to what can be found in the literature. In [7], chiral perturbation theory for N_f quarks in the adjoint representation has been constructed. In this case the symmetry breaking pattern is given by $SU(2N_f) \rightarrow SO(2N_f)$. Notice that for any number of flavors the symmetry breaking pattern of the staggered fermion action is $U(2N_f) \rightarrow SO(2N_f)$.

Following [7, 23], we construct the low-energy effective Lagrangian for the Goldstone modes induced by the spontaneous symmetry breaking $U(2) \rightarrow U(1)$. We find that the effective Lagrangian is given by

$$\mathcal{L}_{\text{eff}} = \frac{F^2}{2} \text{Tr} \nabla_\nu \Sigma \nabla_\nu \Sigma^\dagger - F^2 M_\pi^2 \text{ReTr} \hat{M}_\phi \Sigma, \quad (\text{A1})$$

where F is the pion decay constant, $M_\pi^2 = \sqrt{m^2 + \lambda^2} \langle \bar{\psi} \psi \rangle_0 / 2F^2$, and $\langle \bar{\psi} \psi \rangle_0$ is the quark-antiquark condensate at $m = \lambda = \mu = 0$.

We have used the same conventions as in [7]. These notations were already introduced in section 3, we just need to replace Σ_l by Σ in the expressions that appear in section 3, with

$$\Sigma = U \bar{\Sigma} U^T, \quad (\text{A2})$$

where

$$U = \exp \left(\frac{i\Pi}{2\sqrt{2}F} \right) \quad \text{with} \quad \Pi = \begin{pmatrix} P_S & Q_R + iQ_I \\ Q_R - iQ_I & P_S \end{pmatrix}, \quad (\text{A3})$$

and

$$\bar{\Sigma} = \begin{pmatrix} i \sin \alpha & \cos \alpha \\ \cos \alpha & i \sin \alpha \end{pmatrix}, \quad (\text{A4})$$

corresponds to the minimum of the free energy with α given by

$$4\mu^2 \cos \alpha \sin \alpha = M_\pi^2 \sin(\alpha - \phi). \quad (\text{A5})$$

We now turn to the study of the spectrum. All the computations made in [7] can be easily implemented in our case, since our effective Lagrangian is very similar to that studied in [7].

First at $\mu = 0$, we find that the mass of the three pseudo-Goldstone modes is given by M_π . At $\mu \neq 0$, we can expand the effective Lagrangian (A1) to second order in the Goldstone fields.

Following [7], we find that the term quadratic in the Goldstone fields in the effective Lagrangian is given by

$$\begin{aligned} \mathcal{L}_{\text{eff}} = & \text{Tr} \left[\left(\partial_\nu Q_R^\dagger \partial_\nu Q_R + \partial_\nu Q_I^\dagger \partial_\nu Q_I \right) - 4\mu \cos \alpha \left(Q_I^\dagger \partial_0 Q_R + Q_R^\dagger \partial_0 Q_I \right) \right] \\ & + M_\pi^2 \text{Tr} \left[Q_I Q_I^\dagger \frac{\sin \phi}{\sin \alpha} + Q_R Q_R^\dagger \left(\frac{4\mu^2}{M_\pi^2} \sin^2 \alpha + \frac{\sin \phi}{\sin \alpha} \right) \right] \\ & + \text{Tr} \left[\partial_\nu P_S \partial_\nu P_S + P_S^2 M_\pi^2 \left(\frac{4\mu^2}{M_\pi^2} \cos^2 \alpha + \frac{\sin \phi}{\sin \alpha} \right) \right]. \end{aligned} \quad (\text{A6})$$

The Q and Q^\dagger modes are mixed. If we call \tilde{Q} and \tilde{Q}^\dagger the eigenmodes, we find that the dispersion laws for the different Goldstone modes are given by

$$\begin{aligned} P_S : E^2 = & \mathbf{p}^2 + M_\pi^2 \left(\frac{4\mu^2}{M_\pi^2} \cos^2 \alpha + \frac{\sin \phi}{\sin \alpha} \right); \\ \tilde{Q}^\dagger : E^2 = & \mathbf{p}^2 + M_\pi^2 \frac{\sin \phi}{\sin \alpha} + 2\mu^2(1 + 3 \cos^2 \alpha) \\ & + 2\mu \sqrt{\mu^2(1 + 3 \cos^2 \alpha)^2 + 4 \cos^2 \alpha \left(\mathbf{p}^2 + M_\pi^2 \frac{\sin \phi}{\sin \alpha} \right)}; \\ \tilde{Q} : E^2 = & \mathbf{p}^2 + M_\pi^2 \frac{\sin \phi}{\sin \alpha} + 2\mu^2(1 + 3 \cos^2 \alpha) \\ & - 2\mu \sqrt{\mu^2(1 + 3 \cos^2 \alpha)^2 + 4 \cos^2 \alpha \left(\mathbf{p}^2 + M_\pi^2 \frac{\sin \phi}{\sin \alpha} \right)}. \end{aligned} \quad (\text{A7})$$

-
- [1] R. Rapp, T. Schafer, E.V. Shuryak and M. Velkovsky, Phys. Rev. Lett. **81**, 53 (1998).
[2] M. Alford, K. Rajagopal and F. Wilczek, Phys. Lett. **B422**, 247 (1998).
[3] D. Bailin and A. Love, Phys. Rept. **107**, 325 (1984).

- [4] B. C. Barrois, Nucl. Phys. B219, 390 (1977)
- [5] Z. Fodor and S. D. Katz, Phys. Lett. B534, 87 (2002); Z. Fodor and S. D. Katz, JHEP 03, 014 (2002); S. Choe, et al., Phys. Rev. D65, 054501 (2002); C. R. Allton, et al., Phys. Rev. D66, 074507 (2002); P. de Forcrand and O. Philipsen, eprint hep-lat/0205016 (2002); P. R. Crompton, Nucl. Phys. B619, 499 (2001); P. R. Crompton, Nucl. Phys. B626, 228 (2002).
- [6] J.B. Kogut, M.A. Stephanov and D. Toublan, Phys. Lett. **B464**, 183 (1999).
- [7] J. B. Kogut, M. A. Stephanov, D. Toublan, J. J. Verbaarschot and A. Zhitnitsky, Nucl. Phys. B **582**, 477 (2000).
- [8] K. Splittorff, D. Toublan and J. J. Verbaarschot, Nucl. Phys. B **620**, 290 (2002);
- [9] Nucl. Phys. B **639**, 524 (2002).
- [10] K. Splittorff, D. T. Son and M. A. Stephanov, Phys. Rev. D **64** (2001) 016003.
- [11] B. Vanderheyden and A. D. Jackson, Phys. Rev. D **64**, 074016 (2001).
- [12] S. Hands, J. B. Kogut, M. P. Lombardo and S. E. Morrison, Nucl. Phys. B **558**, 327 (1999) [arXiv:hep-lat/9902034].
- [13] S. Hands, J.B. Kogut, S.E. Morrison and D.K. Sinclair, Nucl. Phys. Proc. Suppl. **94**, 457 (2001). J.B. Kogut, D.K. Sinclair, S. Hands, and S.E. Morrison, Phys. Rev. D64, 094505 (2001).
- [14] J. B. Kogut, D. Toublan and D. K. Sinclair, Phys. Lett. B **514**, 77 (2001) [arXiv:hep-lat/0104010].
- [15] J. B. Kogut, D. Toublan and D. K. Sinclair, Nucl. Phys. B **642**, 181 (2002) [arXiv:hep-lat/0205019].
- [16] J. B. Kogut, D. Toublan and D. K. Sinclair, arXiv:hep-lat/0208076.
- [17] R. Aloisio, V. Azcoiti, G. Di Carlo, A. Galante and A. F. Grillo, Phys. Lett. B493, 189 (2000); R. Aloisio, V. Azcoiti, G. Di Carlo, A. Galante and A. F. Grillo, Nucl. Phys. B606, 322 (2001).
- [18] A. Nakamura, Phys. Lett. 149B, 391 (1984); S. Muroya, A. Nakamura and C. Nonaka, eprint nucl-th/0111082 (2001); Y. Liu, *et al.*, hep-lat/0009009 (2000); see also M. P. Lombardo, hep-lat/9907025 (1999).
- [19] G. Ecker, "Chiral perturbation theory," CERN-TH-6660-92; *In the proceedings of 4th Hellenic School on Elementary Particle Physics, Corfu, Greece, 2-20 Sep 1992 and Lectures given at Cargese Summer School on Quantitative Particle Physics, Cargese, 20 Jul-1 Aug 1992*

- [20] J. B. Kogut and D. K. Sinclair, *Phys. Rev. D* **66**, 014508 (2002) [arXiv:hep-lat/0201017].
- [21] J. B. Kogut and D. K. Sinclair, *Phys. Rev. D* **66**, 034505 (2002) [arXiv:hep-lat/0202028].
- [22] D. T. Son and M. A. Stephanov, *Phys. Rev. Lett.* **86**, 592 (2001); D. T. Son and M. A. Stephanov, *Yad. Fiz.* **64**, 899 (2001), *Phys. Atom. Nucl.* **64**, 834 (2001).
- [23] J. Gasser and H. Leutwyler, *Nucl. Phys. B* **250**, 465 (1985).